Inversion Modeling of Chlorophyll Fluorescence Parameters in Cotton Canopy via Moisture Data and Spectral Analysis

Fuqing Li [1,2], Caiyun Yin [3], Zhen Li [1,2], Jiaqiang Wang [1,2,4,*], Long Jiang [3], Buping Hou [1,2] and Jing Shi [1,2]

1   College of Agriculture, Tarim University, Alar 843300, China; 10757231022@stumail.taru.edu.cn (F.L.);
    120230073@taru.edu.cn (Z.L.); 10757222021@stumail.taru.edu.cn (B.H.);
    10757222033@stumail.taru.edu.cn (J.S.)
2   Key Laboratory of Genetic Improvement and Efficient Production for Specialty Crops in Arid Southern
    Xinjiang of Xinjiang Corps, Alar 843300, China
3   Agricultural Technology Extension Station of the First Division of Xinjiang Production and Construction
    Corps, Alar 843300, China; 120050027@taru.edu.cn (C.Y.); 10757222019@stumail.taru.edu.cn (L.J.)
4   Research Center of Oasis Agricultural Resources and Environment in Southern Xinjiang, Tarim University,
    Alar 843300, China
*   Correspondence: wjqzky@taru.edu.cn

Abstract: The study of chlorophyll fluorescence parameters is very important for understanding plant photosynthesis. Monitoring cotton chlorophyll fluorescence parameters via spectral technology can aid in understanding the photosynthesis, growth, and stress of cotton fields in real time and provide support for cotton growth regulation and planting management. In this study, cotton plot experiments with different water treatments were set up to obtain the spectral reflectance of the cotton canopy, the maximum photochemical quantum yield (Fv/Fm), and the photochemical quenching coefficient (qP) of leaves at different growth stages. Support vector machine regression (SVR), random forest regression (RFR), and artificial neural network regression (ANNR) were used to establish a fluorescence parameter inversion model of the cotton canopy leaves. The results show that the original spectrum was transformed by multivariate scattering correction (MSC), the standard normal variable (SNV), and continuous wavelet transform (CWT), and the model constructed with Fv/Fm passed accuracy verification. The SNV-SVR model at the budding stage, the MSC-SVR model at the early flowering stage, the SNV-SVR model at the full flowering stage, the MSC-SVR model at the flowering stage, and the CWT-SVR model at the full boll stage had the highest estimation accuracy. The accuracies of the three spectral preprocessing and qP models were verified, and the MSC-SVR model at the budding stage, SNV-SVR model at the early flowering stage, MSC-SVR model at the full flowering stage, SNV-SVR model at the flowering stage, and CWT-SVR model at the full boll stage presented the highest estimation accuracies.

Keywords: hyperspectral; chlorophyll fluorescence parameters; cotton

1. Introduction

China leads the world in cotton production, but it is mainly grown in dry areas, with Xinjiang, the core producing region, being particularly affected by drought. Given the shortage of water resources, it is necessary to explore the efficient use of water resources to ensure the high yield and quality of agriculture. Water stress severely affects agricultural production, especially cotton growth [1]. Chlorophyll fluorescence parameters can reveal the internal mechanisms of plant photosynthesis and the physiological state of plants, which is an indispensable indicator in the study of adverse stress. In addition, as a link between plants and the environment, chlorophyll fluorescence parameters are highly important for exploring the relationship between plant photosynthesis and the environment [2]. Among them, Fv′/Fm′ is expressed as the PSII effective photochemical quantum yield, which is highly important for the study of crop physiological changes

and stress [3]. Through changes in physiological indices, the water stress and water demand of cotton can be monitored and diagnosed in a timely and accurate manner, which is highly important for improving cotton water management and guiding water-saving agricultural production [4]. With the rapid development of modern information technology and spectroscopic technology, remote sensing technology has been widely used to monitor photosynthetic parameters and chlorophyll fluorescence indices [5,6]. Leaf chlorophyll provides useful information for carbon, water, and energy exchange between plants and the environment [7] and affects the photosynthetic potential and net primary productivity of plants [8,9]. Chlorophyll content is an important indicator of nutrient stress and plant diseases, which can theoretically guide the precise management of orchards. In addition, it is a key parameter for predicting fruit ripeness and harvest time [10]. Leaf chlorophyll is one of the main storage units of nitrogen in plants [11] and directly affects the nutritional status of plants. Chlorophyll can absorb energy through three pathways, namely, photosynthetic electron transport, chlorophyll fluorescence, and heat dissipation [12], and the chlorophyll fluorescence index of plant leaves can better reflect the changing characteristics of photosynthesis. Pérez-Priego et al. [13] used a PAM-2100 fluorometer (Heinz Walz GmbH, Nuremberg, DE) to determine the diurnal steady state of chlorophyll fluorescence in field leaves and studied the effect of water stress on chlorophyll fluorescence. Ding et al. [14] used a PAM-2100 chlorophyll fluorometer to measure the chlorophyll fluorescence parameters Fv/Fo, Fv/Fm, Fo, and Fm of the top two leaves of cotton plants, and the parameters gradually decreased with increasing cotton fertility, and reasonable nitrogen application increased the potential activity of PSII and the photochemical efficiency of PSII in cotton leaves. Hyperspectral remote sensing technology originated in 1970 and can be used in precision agriculture technology to obtain farmland data, monitor crop habitat, and achieve sustainable agricultural development [15,16]. Vegetation has unique spectral characteristics that can reflect various physiological and morphological characteristics of green plants; thus, the spectral characteristics of crops can be used to monitor their water demand and physiological changes, which can be used as an important basis for vegetation remote sensing monitoring [17]. Chlorophyll fluorescence parameters can reflect the "intrinsic" characteristics of plants, which are called intrinsic probes of the relationship between photosynthesis and the environment [18]. With the rapid development of modern information technology and spectroscopic technology, remote sensing technology has been widely used to monitor chlorophyll fluorescence indicators.

Owing to its advantages of being nondestructive, fast, and highly accurate, spectroscopy technology has been widely used in the monitoring of the physiological state of various crops [19,20]. Previous studies have shown the potential of hyperspectral data and chlorophyll fluorescence indicators in monitoring crop stress [21,22]. Zhang et al. [23] studied the variation in chlorophyll fluorescence with a salinity gradient in *Suaeda salaeda* leaves. To select the sensitive hyperspectral range of leaf chlorophyll fluorescence, the correlation between leaf chlorophyll fluorescence and hyperspectral reflectance was regressed, and they reported that wavelengths of 680 nm and 935 nm were the most sensitive hyperspectral bands for estimating leaf chlorophyll fluorescence. Winkel et al. [24] significantly correlated the PRI (photochemical reflectance index) of quinoa plants with predawn leaf water potential, Fm' and noon Fv/Fm, indicating that PRI and Chl fluorescence are helpful in evaluating the physiological changes in quinoa plants at different developmental stages and under different water conditions. Zarco et al. studied the diurnal variation in leaf reflectance spectra, and in combination with the fluorescence measurements of the PAM-2000 fluorometer, the diurnal variation in leaf reflectance spectra was consistent with the observed diurnal variation in steady-state fluorescence. In this study, the effects of spectral pretreatment technology and an inversion model on fluorescence parameters are discussed. Three pretreatment technologies, MSC, SNV, and CWT, and three inversion models, SVR, RFR, and ANNR, were selected. Two parameters, Fv/Fm and qP, were studied. First, the spectral data were preprocessed, and then three inversion models were applied to the modeling. The results showed that CWT pretreatment combined with the

SVR model had the best ability to predict fluorescence parameters, and the combination of CWT treatment and the SVR model had a stronger ability to predict fluorescence parameters. Moreover, different models gave different performances in different fluorescence parameter analyses. The results show that the accuracy and reliability of fluorescence parameter analysis can be significantly improved by selecting appropriate pretreatment methods and inversion models, and future research can be extended to more fluorescence parameters and practical applications.

2. Materials and Methods

2.1. Overview of the Study Area

This experiment was conducted in 2022 at the National Field Scientific Observation and Research Station of the Aksu Farmland Ecosystem, Chinese Academy of Sciences (80°49′ E, 40°37′ N). The site is in the Tarim Basin of China, which is a typical warm temperate, extreme continental, arid desert climate region. Summers are hot, winters are cold, sunshine hours are abundant, precipitation is scarce, and evaporation is strong. The altitude of the site is 1030 m above sea level. The annual average temperature in this area is 11.2 °C, the average annual precipitation is 45.2 mm, the frost-free period is 211 days, and the annual sunshine duration is 2940 h. Cotton in this area depends on irrigation, and the main water sources are the Aksu River and Tarim River. The climate and extensive cultivation make the area prone to drought. Water stress affects the physiological and fluorescence parameters of cotton. Drought causes chlorophyll decomposition, inhibits photosynthesis, and decreases the fluorescence parameters. Some parameters can be restored after rehydration, but most of them cannot be completely restored. Cotton drip irrigation in Xinjiang requires 6000 cubic meters of water per hectare, which can be reduced to 4200 cubic meters under specific conditions, such as the Bozhou reclamation area, to save water resources. Therefore, five irrigation gradients were set in this experiment to simulate water stress, and their gradients were 900 m^3/hm^2 (W_1), 1800 m^3/hm^2 (W_2), 2700 m^3/hm^2 (W_3), 3600 m^3/hm^2 (W_4), and 4500 m^3/hm^2 (W_5). Experiments were carried out under the conditions of 2400 m^3/hm^{-2} winter irrigation water. A total of 6 periods of irrigation and 5 periods of sampling were assessed in this experiment. Each sampling date was about 10–12 days after the end of watering, and the final sampling dates were 25 June, 6 July, 19 July, 7 August, and 30 August, respectively. The last irrigation date was 5 September and no samples were taken. The actual water depth of each irrigation was 6.67 mm (W_1), 13.34 mm (W_2), 20.01 mm (W_3), 26.68 mm (W_4), and 33.35 mm (W_5). The cotton variety was Tahe No. 2, which was sown on demand with film mulch and drip irrigation under the film. The fluorescence parameters and hyperspectral reflectance of the cotton leaves were measured at the bud stage (BS), early flowering stage (EF), full flowering stage (FB), flowering boll stage (FBS), and boll stage (PBP).

2.2. Fluorescence Data Acquisition

This assay was performed via a PAM-2100 chlorophyll fluorometer. Water stress can reduce the chlorophyll fluorescence parameters of cotton leaves, such as the Fv/Fm and qP, reflecting their physiological status. The dark adaptation time is key for ensuring accurate and reliable data, and 30 min is usually chosen because it balances the physiological needs of the plant, the ease of experimental operation, and the reliability of the data. When measuring, the inverted three or inverted four leaves on the top of the cotton plant, which are active in photosynthesis and can represent the overall physiological state of the plant, were selected. Therefore, when the chlorophyll fluorescence parameters of three or four inverted leaves of labeled cotton plants are measured, dark adaptation should be performed on the leaves for 30 min before different growth periods. The chlorophyll fluorescence parameters of the inverted third or fourth leaves of the labeled cotton plants were measured, the Fv/Fm and qP were measured at different growth stages, and each leaf was darkly adapted for 30 min before the measurement. Fv/Fm was proposed by Demming et al. in 1996 to estimate the relative fraction of the light energy absorbed by the photosynthetic

mechanism for photochemical reactions and heat dissipation of the antenna [25]; qP is an indicator of the proportion of open reaction centers in PSII and the ability of captured photon energy to be used for photochemical reactions [26].

2.3. Spectral Data Acquisition

In this study, a PSR-1100 portable object spectrometer (Spectral Evolution, Haverhill, MA, USA) was used to measure the spectral reflectance of the blades. The experimental conditions were windless and clear with the sky being less than 20% cloudy from 11:30 to 16:30. To improve accuracy, enhance reliability, improve repeatability, speed up the discovery of rules, and reduce costs in this study, 15 cotton plants with similar growth conditions and healthy plants or diseases were selected, 3–4 representative functional leaves were selected from different parts of each cotton plant as samples, and three repeated measurements were carried out. The measurement band range was 320–1100 nm, and the spectral resolution was 1 nm. After the spectral reflectance of the blade was measured, the outliers were eliminated, and the average value of the remaining data was taken as the spectral reflectance value of the point. Twenty spectral reflectance curves were obtained at each growing site. Before measurement, whiteboard calibration was required to solve problems such as drift and sensitivity decline, which may occur after the instrument is used for a long time, to ensure the accuracy and reliability of the measuring instrument.

2.4. Spectral Data Preprocessing

In spectral pretreatment, the MSC, SNV, and CWT are used to improve the quality of the spectral data, which is conducive to accurate estimation of the fluorescence parameters. MSC eliminates system variation by standardizing data, SNV removes scattering and background interference, and CWT helps identify and remove noise by breaking down signals. These methods work together to improve the stability and accuracy of spectral data and are suitable for accurate fluorescence parameter estimation.

Competitive adaptive reweighted sampling (CARS) and the continuous projection algorithm (SPA) are two methods for selecting variables in spectral data. CARS simplifies the model by eliminating unimportant variables, whereas SPA selects key variables via projection. When used alone, CARS may ignore important variables, and SPA may be affected by multicollinearity. Combining CARS and SPA can improve model performance by first reducing variables with CARS and then selecting key variables with SPA. In spectral analysis, the combined use of CARS-SPA is more effective than the use of CARS-SPA alone, improving predictive performance, simplifying models, ensuring stability, and overcoming the limitations of each approach.

Therefore, the preprocessed spectral data, Fv/Fm, and qP, were screened via CARS-SPA, and the optimal variable subset was selected to extract the feature bands.

2.5. Modeling Methods

The extracted feature bands were used as input variables, and support vector machine regression (SVR), random forest regression (RFR), and artificial neural network regression (ANNR) methods were used to establish an inversion model of the fluorescence parameters of the cotton canopy leaves. SVR is a pattern recognition method based on statistical learning theory. It is a machine learning algorithm developed by Vladimir Vapnik for classification or regression, including linear and nonlinear regressions. In this study, a support vector machine linear regression function was used [27]. The advantages of RFR are high accuracy, stability, ability to handle high-dimensional data, and the efficiency of parallel processing. RFR is an ensemble learning-based algorithm that performs regression tasks by building multiple decision trees and integrating their predictions. In a random forest, each decision tree is independent and trained on randomly selected subsamples, which can effectively reduce the risk of overfitting [28]. ANNR is known for its powerful nonlinear modeling capabilities, adaptive learning ability, and wide range of applications. The choice of model should be based on specific application scenarios and requires a method

based on gradient learning, which is a nonparametric nonlinear model that uses neural networks to propagate between layers to simulate human brain receivers and information processing [29]. Since weather changes in Xinjiang are not obvious and precipitation is low, the influences of other variables, such as environmental factors, on the inversion model were not considered.

2.6. Accuracy Evaluation

In this experiment, we used the coefficient of determination R^2, root mean square error (RMSE), and relative analysis error (RPD) to evaluate the accuracy of each model. In general, larger R^2 and RPD values correspond to smaller RMSEs, which indicates that the simulation results have high accuracy. R^2 is used to measure the closeness of the correlation, whereas RMSE is used to measure the degree of deviation between the estimate and the true value. If the RMSE value is small, the degree of deviation is low. In other words, the closer R^2 is to 1, the smaller the RMSE and the larger the RPD are, indicating that the model built is more accurate. When the RPD value is between 1.6 and 2.0, the accuracy of the model is acceptable. When the RPD value is greater than 2.0, the constructed model has high reliability. By comparing the values of R^2, RMSE, and RPD of the inversion model, we can select the optimal inversion model.

The formulas for R^2, RMSE, and RPD are expressed as follows [30]:

$$R^2 = \left(1 - \frac{\sum_{i=1}^{n}(y_i - x_i)^2}{\sum_{i=1}^{n}(y_i - \overline{y})^2} \right) \tag{1}$$

$$RMSE = \sqrt{\frac{\sum_{i=1}^{n}(x_i - y_i)^2}{n}} \tag{2}$$

$$SD = \sqrt{\frac{\sum_{i=1}^{n}(y_i - \overline{y}_i)^2}{n-1}} \tag{3}$$

$$RPD = \frac{SD}{RMSE} \tag{4}$$

where x_i and y_i are the simulated and measured fluorescence feature parameter values, respectively, $\overline{y}$ is the average value of the measured fluorescence feature parameters, and n is the number of samples.

3. Results

3.1. Variation Characteristics of Chlorophyll Fluorescence

The chlorophyll fluorescence parameters of the cotton canopy leaves at different key growth stages were studied under different irrigation treatments, and their chemical characteristics are shown in Figure 1.

Figure 1a shows the Fv/Fm changes in cotton at different growth stages under different water treatments. During the BS period, with increasing irrigation, the Fv/Fm ratio first increased but then decreased, and that in the W_4 treatment was the greatest. The trend was similar to that of the EF, PBP, and BS periods. During the FB period, the Fv/Fm ratio first decreased, then increased and then decreased, and W_4 presented the greatest decrease. During the FBS period, the Fv/Fm first increased, then decreased and then increased, and the W_2 treatment had the greatest effect. Drought reduced the Fv/Fm value, indicating that water has an important effect on photosynthesis. Figure 1b shows changes in the qP of cotton at different growth stages under different water treatments. During the BS period, the qP first decreased but then increased with increasing irrigation amount, and that in the W_1 treatment was the highest. During the EF and FB periods, qP decreased with increasing irrigation amount. During the FBS and PBP periods, the changes in qP were complex and related to changes in leaf senescence and photosynthesis. In summary, cotton has different water requirements at different growth stages, and an appropriate amount of water is

conducive to photosynthesis. Too much or too little water may have adverse effects. Under drought conditions, photosynthesis is impaired, and the values of chlorophyll fluorescence parameters are restricted.
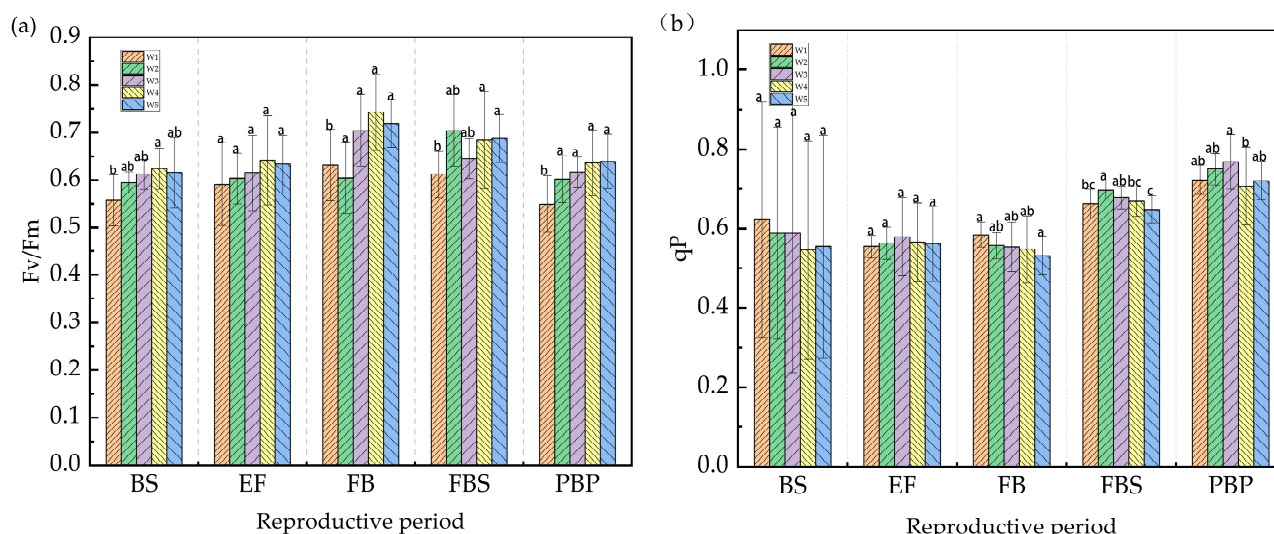
Figure 1. Changes in the chlorophyll fluorescence parameters of cotton leaves at different growth stages. (**a**) Fv/Fm changes at different growth stages, (**b**) qP changes at different growth stages. (In the figure, a, b, c, ab and bc are the letter marking methods for significance analysis. If they do not contain the same letters, there is a significant difference).

The 5 treatments were performed in 15 replicates, with 20 replicates in the W_1 and W_2 treatments, 5 replicates in W_3, 15 replicates in the W_4 and W_5 treatments, and 10 replicates in each treatment during the EF period. The Fv/Fm content data of a total of 320 samples were statistically analyzed according to different water treatments, and the results are shown in Table 1.

Table 1 indicates that the cotton leaf Fv/Fm content varied widely across the treatments, meeting the data requirements. The Fv/Fm content in cotton leaves under different water treatments mostly varied slightly, with moderate variability at the EF and FB stages and less variation in the W_3 and W_5 treatments. These findings suggest inhibited growth under drought stress and vigorous growth at the FB and FBS stages. The highest Fv/Fm content was detected in the W_4 and W_5 treatments, whereas the lowest value was detected in W_1 and W_2, although the difference was not significant. The Fv/Fm content initially increased but then decreased with increasing irrigation, peaking in the W_4 treatment. It reached a maximum during the FBS period and slightly decreased during the PBP period. The results suggest that 3600 m^3/hm^2 irrigation is optimal for cotton growth. The chlorophyll content in the W_1 treatment was significantly lower than that in the other treatments, and that in W_5 was slightly lower than that in W_4, possibly because excess water reduces the chlorophyll content, affects cell metabolism, and reduces the Fv/Fm content.

The 5 treatments were performed in 15 replicates, including 20 replicates for the W_1 and W_2 treatments and 12 replicates for the W_3, W_4, and W_5 treatments during the BS period. The qP content data of a total of 376 samples were statistically analyzed according to different water treatments, and the results are shown in Table 2.

Table 2 shows that the maximum and minimum values of the qP content in cotton leaves are widely distributed, which meets the data requirements. The variability of the qP content in cotton leaves was minimal under the different water treatments but had high variability at the BS stage. During the other growth stages, the variability of each treatment decreased, and the qP content under each irrigation amount increased with the growth of the plants. During the same growth stage, the qP content first increased but then decreased with increasing irrigation amount, reaching a maximum under the W_2 or W_3 treatments.

These findings indicate that the growth of cotton is limited under drought stress. This result suggests that the maximum value under the W_2 or W_3 treatment was slightly greater than that under the other treatments, which may be due to a decrease in chlorophyll content due to insufficient or excessive water, which in turn affects the metabolic and functional disorders of cells, hinders chlorophyll synthesis, and accelerates chlorophyll decomposition, resulting in a decrease in the qP content.

Table 1. Statistical description of the Fv/Fm ratio in cotton leaves at different growth stages under different water treatments.

Method	Irrigation Treatment	Number of Samples	Fv/Fm Content			
			MIN	MAX	Mean	Coefficient
BS	W_1	8	0.44	0.632	0.556	10.3%
	W_2	10	0.544	0.638	0.594	3.9%
	W_3	10	0.551	0.65	0.612	5.4%
	W_4	8	0.577	0.687	0.624	7.4%
	W_5	9	0.457	0.735	0.615	12.7%
EF	W_1	10	0.461	0.723	0.591	15.6%
	W_2	10	0.524	0.705	0.604	9.4%
	W_3	10	0.45	0.711	0.615	13.7%
	W_4	10	0.478	0.789	0.642	15.4%
	W_5	10	0.557	0.727	0.634	10.1%
FBS	W_1	15	0.433	0.714	0.631	12.5%
	W_2	15	0.563	0.808	0.704	11.1%
	W_3	15	0.607	0.758	0.714	6.2%
	W_4	15	0.621	0.86	0.743	11.0%
	W_5	15	0.646	0.805	0.719	7.2%
FB	W_1	15	0.513	0.686	0.612	8.3%
	W_2	15	0.523	0.73	0.637	9.9%
	W_3	15	0.538	0.689	0.645	6.8%
	W_4	15	0.472	0.811	0.684	15.5%
	W_5	15	0.614	0.773	0.687	7.6%
PBP	W_1	15	0.412	0.657	0.549	11.1%
	W_2	15	0.507	0.688	0.602	8.6%
	W_3	15	0.561	0.674	0.616	5.5%
	W_4	15	0.517	0.77	0.636	11.3%
	W_5	15	0.553	0.723	0.639	9.2%

Table 2. Statistical description of the qP content in cotton leaves at different growth stages under different water treatments.

Method	Irrigation Treatment	Number of Samples	qP Content			
			MIN	MAX	Mean	Coefficient
BS	W_1	20	0.101	0.905	0.622	49.2%
	W_2	20	0.118	0.924	0.589	46.5%
	W_3	12	0.113	0.906	0.571	64.4%
	W_4	12	0.159	0.911	0.546	52.6%
	W_5	12	0.125	0.904	0.555	52.8%
EF	W_1	15	0.524	0.615	0.555	5.2%
	W_2	15	0.46	0.627	0.563	7.3%
	W_3	15	0.405	0.764	0.579	17.6%
	W_4	15	0.407	0.697	0.566	18.0%
	W_5	15	0.382	0.661	0.562	17.4%

Table 2. *Cont.*

Method	Irrigation Treatment	Number of Samples	qP Content			
			MIN	MAX	Mean	Coefficient
FBS	W_1	15	0.533	0.668	0.584	5.5%
	W_2	15	0.491	0.624	0.557	6.1%
	W_3	15	0.448	0.705	0.553	11.8%
	W_4	15	0.435	0.782	0.547	15.9%
	W_5	15	0.399	0.603	0.532	9.8%
FB	W_1	15	0.582	0.748	0.663	5.6%
	W_2	15	0.638	0.73	0.696	3.6%
	W_3	15	0.627	0.723	0.678	4.4%
	W_4	15	0.606	0.727	0.668	5.8%
	W_5	15	0.596	0.716	0.648	5.6%
PBP	W_1	15	0.638	0.767	0.723	5.3%
	W_2	15	0.647	0.814	0.75	5.5%
	W_3	15	0.639	0.887	0.768	9.4%
	W_4	15	0.549	0.838	0.707	14.4%
	W_5	15	0.606	0.797	0.721	7.1%

The correlations between the Fv/Fm and qP values at different growth stages and the corresponding irrigation amount were analyzed, and the correlation heatmap of each growth period is shown in Figure 2.
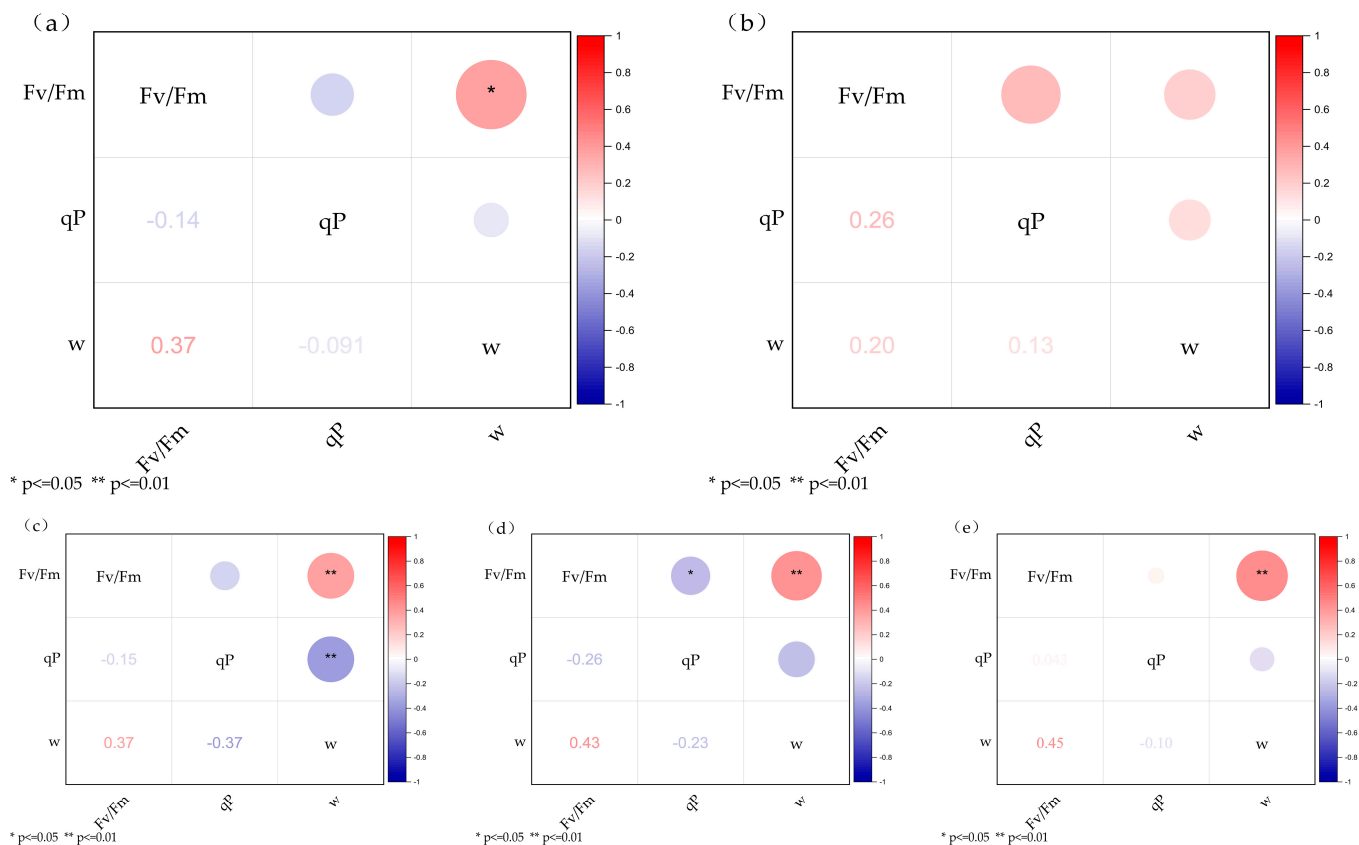
Figure 2. Correlation heatmap of chlorophyll fluorescence parameters with moisture data. (**a**) Heat map of correlation between BS growth period and water data, (**b**) Heat map of correlation between EF growth period and water data, (**c**) Heat map of correlation between FB growth period and water data, (**d**) Heat map of correlation between FBS growth period and water data, (**e**) Heat map of correlation between PBP growth period and water data.

Figure 2 shows the correlation heatmap for different growth periods. As shown in Figure 2a–e, the reproductive periods are BS, EF, FB, FBS, and PBP. As shown in Figure 2a, there was a significant correlation between the Fv/Fm and moisture data, whereas the qP was negatively correlated with the moisture data, but the correlation was not significant. Figure 2b shows that there is a positive correlation between Fv/Fm and qP, but the correlation is not significant. Figure 2c shows that Fv/Fm has a positive correlation with the moisture data and a very significant correlation, whereas qP has a negative correlation with the moisture data. Figure 2d shows that Fv/Fm is positively correlated with the moisture data, with a very significant correlation, and that qP is negatively correlated with the moisture data. Finally, Figure 2e shows that Fv/Fm has a positive correlation with the moisture data, with a very significant correlation, whereas qP has a nonsignificant, negative correlation with the moisture data.

3.2. Filtering of Feature Bands

Spectra for the cotton canopy were 320–1100 nm. To eliminate redundant information and improve modeling efficiency, the CARS and SPA algorithms were used to screen the feature wavelengths, and then the optimal subset of variables was determined to extract the feature bands. The CARS algorithm simulates the principle of "survival of the fittest" in Darwin's theory of evolution by retaining wavelength points with large regression coefficients and eliminating points with small weights through adaptive reweighted sampling technology. On this basis, the combination of variables with small root mean square errors was selected through cross-validation [31]. SPA is a method used to find the group of variables with the lowest redundancy information in the spectral information, and the selection of characteristic wavelengths is realized by comparing the projections of the variables. The algorithm can effectively eliminate the collinearity problem and avoid repeated extraction of overlapping information to achieve good performance in spectral data analysis [32,33].

According to two fluorescence parameters and three spectra, the CARS and SPA algorithms were used to screen the spectral characteristic bands, and a subset of the optimal variables was selected to extract the characteristic bands, among which the CARS algorithm screened more characteristic bands. Then, the SPA algorithm could be used to fix the number of characteristic bands, and 10 subsets of optimal variables were selected to extract the characteristic bands. The characteristic bands of the optimal model after simulation for different growth periods are shown in Table 3.

Table 3. Characteristic bands of the optimal model after simulation of the model at different growth stages.

Reproductive Period	Fluorescence Parameters	Characteristic Bands
BS	Fv/Fm	323, 327, 330, 568, 686, 728, 976, 1047, 1069, 1089
	qP	333, 416, 681, 724, 751, 859, 928, 934, 1078, 1090
EF	Fv/Fm	320, 330, 336, 428, 554, 737, 997, 1058, 1093, 1098
	qP	325, 332, 345, 523, 725, 779, 949, 1063, 1069, 1097
FB	Fv/Fm	320, 337, 511, 585, 675, 931, 982, 1042, 1087, 1100
	qP	323, 342, 586, 685, 738, 920, 1039, 1041, 1069, 1100
FBS	Fv/Fm	344, 397, 432, 508, 688, 700, 718, 958, 970, 1068
	qP	702, 727, 922, 954, 974, 976, 987, 1057, 1066, 1079
PBP	Fv/Fm	377, 747, 782, 821, 853, 855, 959, 968, 1003, 1010
	qP	400, 443, 517, 531, 632, 813, 890, 920, 987, 1100

The correlation analysis between the selected characteristic bands and the corresponding fluorescence parameters at different growth stages is shown in Figure 3.
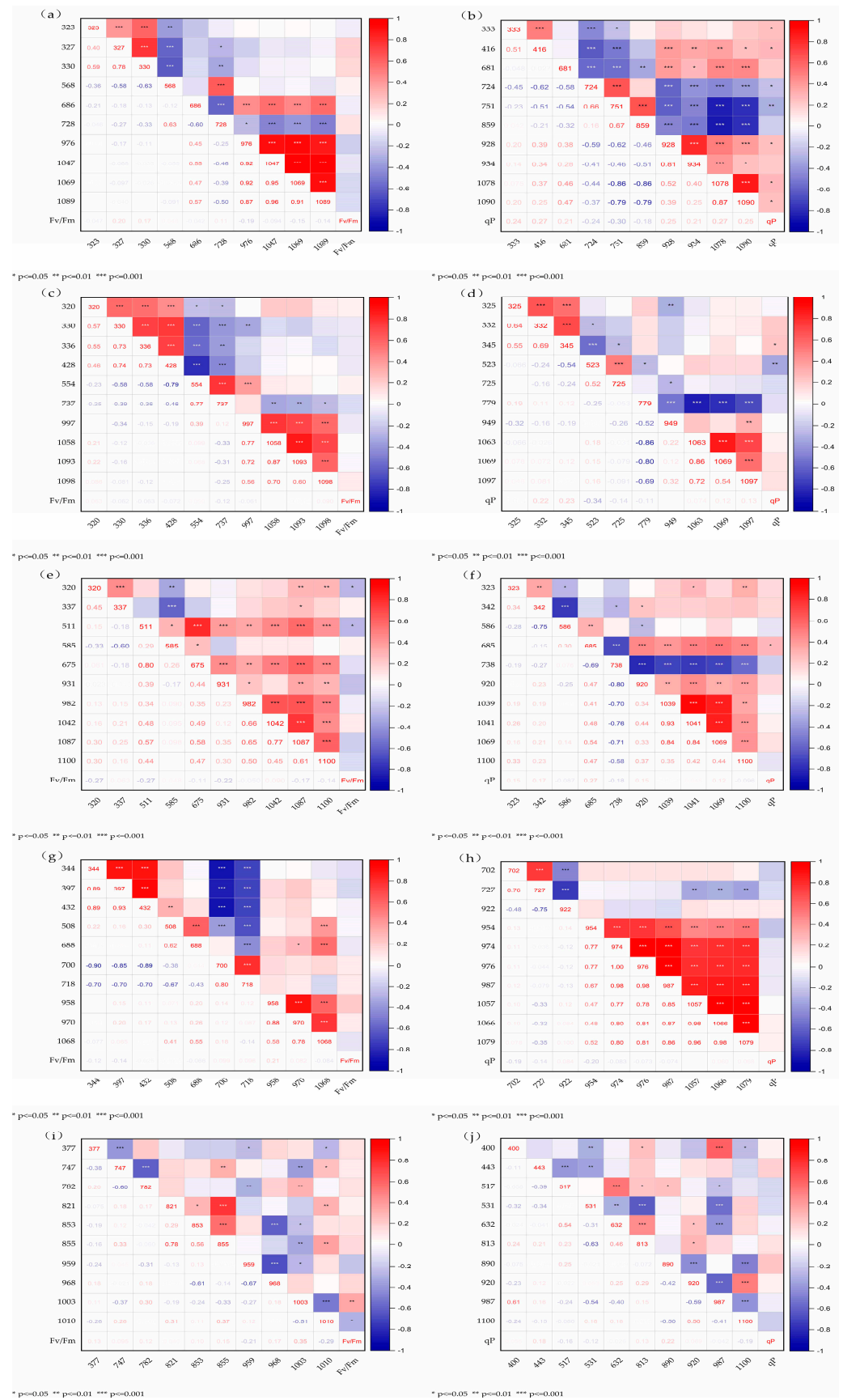
Figure 3. Heatmap of the correlation between characteristic bands and chlorophyll fluorescence characteristic parameters. (**a**) Heat map of correlation between Fv/Fm and characteristic bands during

BS growth period, (**b**) Heat map of correlation between qP and characteristic bands during BS growth period, (**c**) Heat map of correlation between Fv/Fm and characteristic bands during EF growth period, (**d**) Heat map of correlation between qP and characteristic bands during EF growth period, (**e**) Heat map of correlation between Fv/Fm and characteristic bands during FB growth period, (**f**) Heat map of correlation between qP and characteristic bands during FB growth period, (**g**) Heat map of correlation between qP and characteristic bands during FBS growth period, (**h**) Heat map of correlation between qP and characteristic bands during FBS growth period, (**i**) Heat map of correlation between Fv/Fm and characteristic bands during PBP growth period, (**j**) Heat map of correlation between qP and characteristic bands during PBP growth period.

Figure 3a–j shows the correlation heatmap of the optimal bands screened for different growth stages (BS (a,b), EF (c,d), FB (e,f), FBS (g,h), PBP (i,j)) with Fv/Fm and qP. Each stage contains two subplots showing correlations with Fv/Fm and qP. These heatmaps emphasize the close connection between chlorophyll fluorescence parameters and specific light bands in plants at different stages of growth. They verify the effectiveness and reliability of the characteristic bands screened by the CARS-SPA method in a variety of growth environments. These screened bands can accurately reflect the growth status of plants, which provides important data for the study of plant physiology and ecology. In addition, by analyzing these correlation data, we can gain a deeper understanding of how plants adapt to different growth conditions, providing scientific guidance for optimizing the plant growth environment and improving growth efficiency.

3.3. Model Construction and Accuracy Verification

The spectral performance of different transformations is different, and three methods, SVR, RFR, and ANNR, are used to simulate the two fluorescence characteristic parameters, and the accuracy. R^2, RMSE, and RPD are comprehensively modeled and verified, and the simulation results are shown in Tables 4–8. The simulation combinations with the highest comprehensive accuracy of modeling and verification are selected from Tables 4–8 and plotted in scatter plots (Figures 4–8).

Table 4. BS simulates fluorescence signature parameter results via SVR, RFR, and ANNR.

		BS					
		Fv/Fm			qP		
Method	Simulation Results	SVR	RFR	ANNR	SVR	RFR	ANNR
MSC	Modeling R^2	0.656	0.705	0.502	0.918	0.752	0.292
	Modeling RMSE	0.002	0.031	0.032	0.006	0.186	0.245
	Modeling RPD	1.434	0.643	0.993	3.307	0.753	0.849
	Verify R^2	0.610	0.291	0.396	0.653	0.155	0.165
	Verify RMSE	0.002	0.053	0.045	0.013	0.283	0.305
	Verify RPD	1.393	0.336	0.872	1.156	0.459	0.700
SNV	Modeling R^2	0.974	0.708	0.844	0.730	0.824	0.426
	Modeling RMSE	0.010	0.032	0.020	0.005	0.204	0.224
	Modeling RPD	6.176	0.639	2.248	1.496	0.577	0.895
	Verify R^2	0.986	0.258	0.517	0.272	0.520	0.257
	Verify RMSE	0.009	0.049	0.037	0.015	0.228	0.270
	Verify RPD	8.438	0.382	1.338	0.704	0.376	0.813
CWT	Modeling R^2	0.864	0.812	0.815	0.820	0.760	0.267
	Modeling RMSE	0.001	0.029	0.020	0.011	0.203	0.258
	Modeling RPD	2.307	0.901	2.171	1.935	0.601	0.699
	Verify R^2	0.789	0.656	0.603	0.491	0.211	0.398
	Verify RMSE	0.002	0.035	0.039	0.018	0.264	0.229
	Verify RPD	1.808	0.566	1.287	0.934	0.290	0.766

Table 5. EF simulates the results of fluorescence signature parameters via SVR, RFR, and ANNR.

		EF					
		Fv/Fm			qP		
Method	Simulation Results	SVR	RFR	ANNR	SVR	RFR	ANNR
MSC	Modeling R^2	0.885	0.811	0.629	0.435	0.822	0.309
	Modeling RMSE	0.004	0.043	0.052	0.005	0.056	0.065
	Modeling RPD	2.775	0.882	1.577	0.792	0.530	0.660
	Verify R^2	0.816	0.256	0.625	0.001	0.353	0.321
	Verify RMSE	0.005	0.074	0.056	0.012	0.066	0.067
	Verify RPD	2.140	0.348	1.559	0.592	0.275	0.656
SNV	Modeling R^2	0.650	0.823	0.776	0.875	0.838	0.181
	Modeling RMSE	0.004	0.049	0.036	0.018	0.049	0.075
	Modeling RPD	1.293	0.704	2.039	2.459	0.719	0.579
	Verify R^2	0.449	0.513	0.488	0.317	0.185	0.351
	Verify RMSE	0.004	0.058	0.064	0.051	0.073	0.062
	Verify RPD	0.967	0.477	1.161	1.107	0.256	1.024
CWT	Modeling R^2	0.841	0.842	0.697	0.807	0.849	0.580
	Modeling RMSE	0.003	0.045	0.041	0.004	0.056	0.047
	Modeling RPD	1.997	1.068	1.723	1.672	0.561	1.206
	Verify R^2	0.871	0.654	0.641	0.186	0.229	0.153
	Verify RMSE	0.003	0.040	0.057	0.012	0.061	0.086
	Verify RPD	2.306	0.746	1.660	0.597	0.299	0.589

Table 6. FB simulates fluorescence feature parameter results via SVR, RFR, and ANNR.

		FB					
		Fv/Fm			qP		
Method	Simulation Results	SVR	RFR	ANNR	SVR	RFR	ANNR
MSC	Modeling R^2	0.889	0.781	0.541	0.992	0.743	0.391
	Modeling RMSE	0.003	0.045	0.052	0.001	0.045	0.045
	Modeling RPD	2.894	0.670	1.336	11.177	0.497	0.930
	Verify R^2	0.167	0.160	0.119	0.761	0.134	0.243
	Verify RMSE	0.013	0.086	0.102	0.003	0.044	0.057
	Verify RPD	0.513	0.232	0.854	1.937	0.264	0.841
SNV	Modeling R^2	0.912	0.814	0.365	0.930	0.779	0.192
	Modeling RMSE	0.003	0.050	0.054	0.006	0.045	0.051
	Modeling RPD	3.277	0.617	0.765	3.499	0.473	0.568
	Verify R^2	0.514	0.281	0.251	0.638	0.111	0.107
	Verify RMSE	0.009	0.071	0.081	0.016	0.046	0.064
	Verify RPD	0.886	0.230	0.463	1.057	0.292	0.419
CWT	Modeling R^2	0.868	0.779	0.468	0.752	0.771	0.602
	Modeling RMSE	0.004	0.048	0.060	0.004	0.035	0.038
	Modeling RPD	2.379	0.768	1.230	1.513	0.699	1.279
	Verify R^2	0.381	0.278	0.409	0.456	0.253	0.485
	Verify RMSE	0.020	0.065	0.067	0.006	0.059	0.045
	Verify RPD	0.541	0.599	1.171	0.740	0.373	0.926

In Table 4, during the BS growth period, the SVR model simulated Fv/Fm with the spectral expression capability of SNV > CWT > MSC, the RFR model simulated the spectral expression capability of CWT > SNV > MSC, and the ANNR model simulated the spectral expression capability of CWT > SNV > MSC. For the qP simulation, the spectral performance capability of the SVR model is MSC > CWT > SNV, the spectral performance capability of the RFR model is SNV > CWT > MSC, and the spectral performance of the ANNR model is SNV > CWT > MSC.

Table 7. The FBS simulates the fluorescence signature parameter results via SVR, RFR, and ANNR.

		FBS					
		Fv/Fm			qP		
Method	**Simulation Results**	**SVR**	**RFR**	**ANNR**	**SVR**	**RFR**	**ANNR**
MSC	Modeling R^2	0.879	0.829	0.632	0.976	0.665	0.230
	Modeling RMSE	0.005	0.046	0.042	0.002	0.026	0.029
	Modeling RPD	2.774	0.619	1.175	6.165	0.655	0.815
	Verify R^2	0.876	0.145	0.385	0.914	0.134	0.108
	Verify RMSE	0.008	0.069	0.066	0.005	0.030	0.044
	Verify RPD	1.535	0.279	1.049	2.524	0.349	0.610
SNV	Modeling R^2	0.946	0.793	0.375	0.977	0.702	0.268
	Modeling RMSE	0.013	0.049	0.053	0.007	0.025	0.029
	Modeling RPD	4.211	0.645	1.000	6.417	0.574	0.586
	Verify R^2	0.705	0.136	0.274	0.913	0.325	0.344
	Verify RMSE	0.028	0.060	0.076	0.015	0.032	0.036
	Verify RPD	1.488	0.275	0.824	2.997	0.351	0.486
CWT	Modeling R^2	0.845	0.803	0.631	0.870	0.752	0.510
	Modeling RMSE	0.001	0.047	0.043	0.033	0.023	0.028
	Modeling RPD	2.262	0.750	0.109	2.584	0.848	1.287
	Verify R^2	0.397	0.387	0.180	0.828	0.029	0.536
	Verify RMSE	0.001	0.050	0.070	0.060	0.333	0.030
	Verify RPD	1.006	0.533	0.695	1.479	0.612	1.101

Table 8. PBP simulates fluorescence signature parameter results via SVR, RFR, and ANNR.

		PBP					
		Fv/Fm			qP		
Method	**Simulation Results**	**SVR**	**RFR**	**ANNR**	**SVR**	**RFR**	**ANNR**
MSC	Modeling R^2	0.804	0.829	0.274	0.746	0.756	0.437
	Modeling RMSE	0.002	0.035	0.058	0.002	0.045	0.057
	Modeling RPD	1.888	0.961	0.943	1.557	0.677	0.985
	Verify R^2	0.005	0.215	0.437	0.057	0.152	0.304
	Verify RMSE	0.005	0.083	0.053	0.003	0.059	0.057
	Verify RPD	0.464	0.274	1.086	0.433	0.407	1.059
SNV	Modeling R^2	0.593	0.772	0.505	0.922	0.795	0.234
	Modeling RMSE	0.023	0.046	0.041	0.011	0.046	0.063
	Modeling RPD	1.031	0.569	1.052	3.469	0.620	0.754
	Verify R^2	0.033	0.227	0.431	0.446	0.330	0.500
	Verify RMSE	0.068	0.055	0.060	0.026	0.056	0.053
	Verify RPD	0.306	0.371	0.829	0.685	0.327	1.109
CWT	Modeling R^2	0.855	0.827	0.567	0.766	0.818	0.559
	Modeling RMSE	0.001	0.036	0.046	0.004	0.044	0.046
	Modeling RPD	2.370	0.682	1.261	1.732	0.737	0.988
	Verify R^2	0.823	0.228	0.365	0.601	0.465	0.264
	Verify RMSE	0.001	0.072	0.045	0.005	0.049	0.057
	Verify RPD	2.233	0.216	1.000	1.027	0.405	0.800

As shown in Table 4, considering the accuracy and error of modeling and verification, the optimal inversion model combinations of Fv/Fm and qP during the BS growth period are the SVR model based on the CWT and the SVR model based on the MSC. The scatter plot of the optimal model is shown in Figure 4.
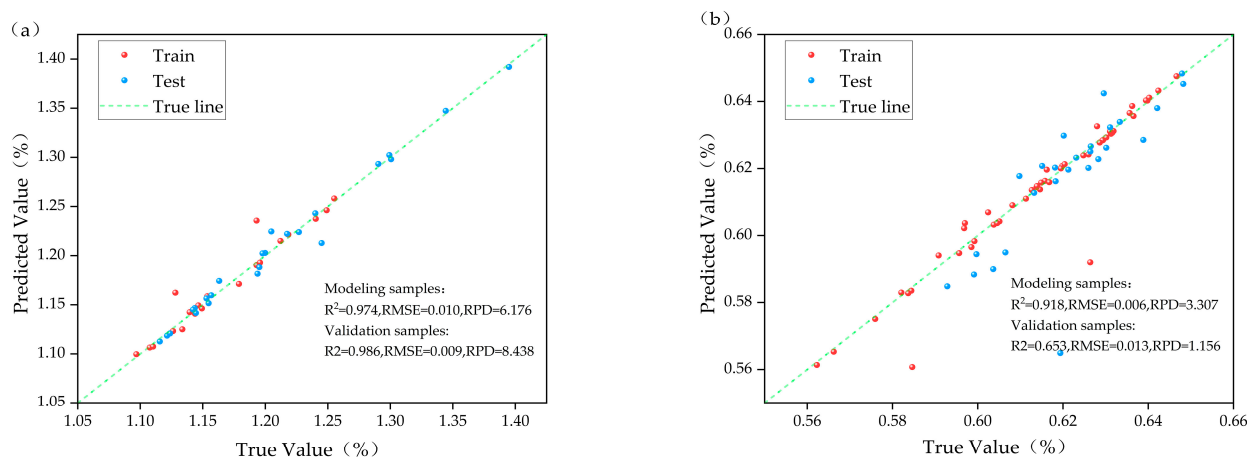
Figure 4. Scatter plots of the optimal simulated and measured values of Fv/Fm (**a**) and qP (**b**) during the BS period.

In Figure 4, the modeling R^2 values are 0.974 and 0.918, the verification R^2 values are 0.986 and 0.653, the modeling RMSE values are 0.010 and 0.006, the verification RMSE values are 0.009 and 0.013, the modeling RPD values are 6.176 and 3.307, and the verification RPD values are 8.438 and 1.156.

In Table 5, during the growth period of the EF, the SVR model simulated Fv/Fm, and the spectral performance ability was as follows: MSC > CWT > SNV. In the RFR model simulation, the spectral performance ability was CWT > SNV > MSC. In the ANNR model simulation, the spectral performance capability was CWT > MSC > SNV. For the qP simulation, the spectral performance ability of the SVR model is as follows: SNV > CWT > MSC. When the RFR model was simulated, the spectral performance ability was as follows: SNV > CWT > MSC. When the ANNR model was simulated, the spectral performance ability was CWT > MSC > SNV.

As shown in Table 5, considering the accuracy and error of modeling and verification, the optimal inversion model combinations of Fv/Fm and qP during EF fertility were the MSC-based SVR model and the SNV-based SVR model, respectively. The scatter plot of the optimal model is shown in Figure 5.
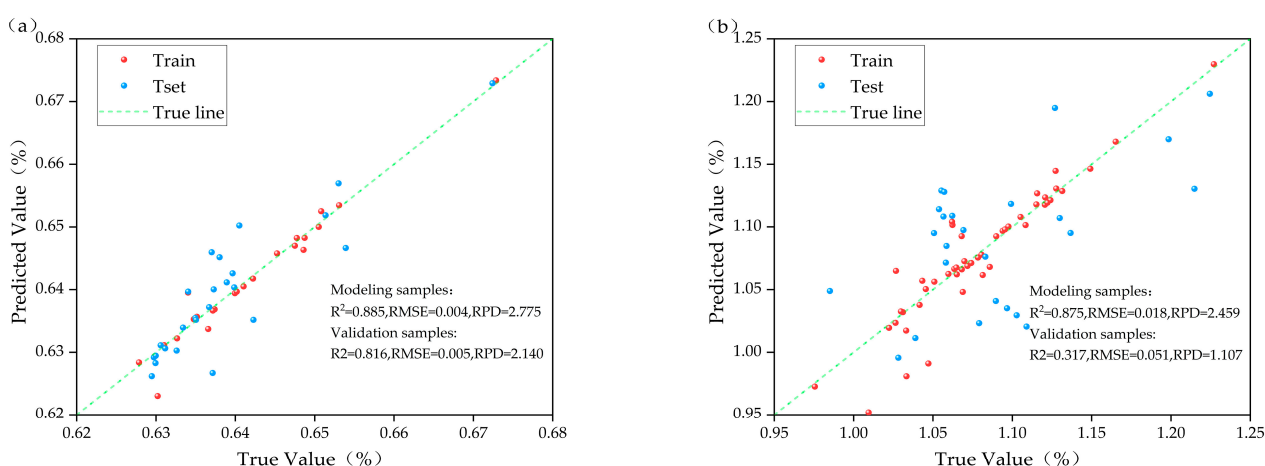
Figure 5. Scatter plots of the optimal simulated and measured values of Fv/Fm (**a**) and qP (**b**) in the EF period.

In Figure 5, the modeled R^2 values are 0.885 and 0.875, the verified R^2 values are 0.816 and 0.317, the modeled RMSE values are 0.004 and 0.018, the verified RMSE values are 0.005 and 0.051, the modeling RPD values are 2.775 and 2.459, and the verified RPD values are 2.140 and 1.107.

In Table 6, during the growth period of the FB, the SVR model simulated Fv/Fm, and the spectral expression ability was as follows: SNV > CWT > MSC. In the RFR model simulation, the spectral performance ability was SNV > CWT > MSC. In the ANNR model simulation, the spectral performance capability was CWT > MSC > SNV. For the qP simulation, the spectral performance ability of the SVR model was as follows: MSC > SNV > CWT. When the RFR model was simulated, the spectral performance ability was as follows: CWT > MSC > SNV. When the ANNR model was simulated, the spectral performance ability was CWT > MSC > SNV.

As shown in Table 6, considering the accuracy and error of modeling and validation, the optimal inversion model combinations of Fv/Fm and qP during FB fertility are the SNV-based SVR model and the MSC-based SVR model, respectively. The scatter plot of the optimal model is shown in Figure 6.
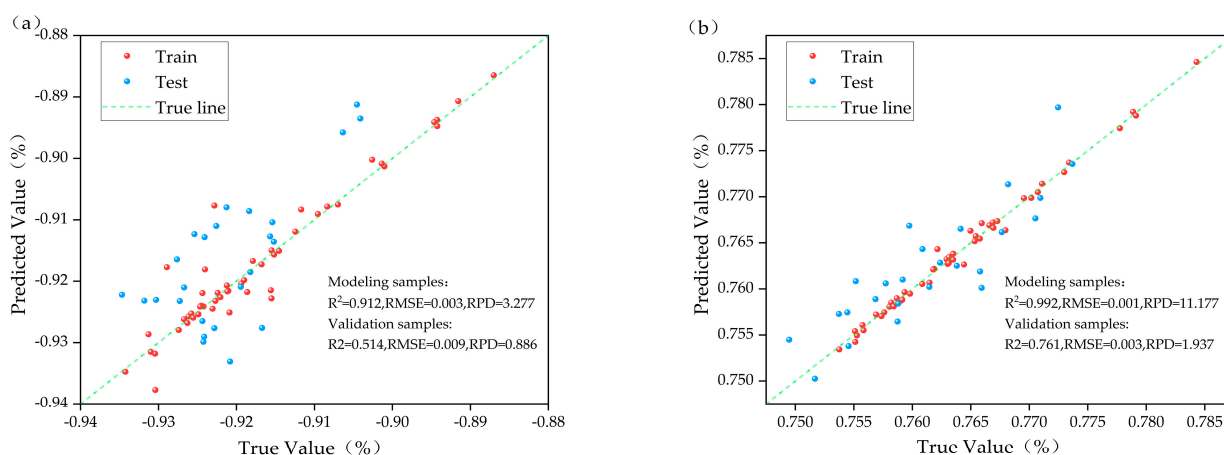
Figure 6. Scatter plots of the optimal simulated and measured values of Fv/Fm (**a**) and qP (**b**) during the FB period linearly fitted to the measured values.

In Figure 6, the modeled R^2 values are 0.912 and 0.992, the verification R^2 values are 0.514 and 0.761, the modeling RMSE values are 0.003 and 0.001, the verification RMSE values are 0.009 and 0.003, the modeling RPD values are 3.277 and 11.177, and the verification RPD values are 0.886 and 1.937.

In Table 7, during the FBS growth period, the SVR model simulated Fv/Fm, and the spectral performance ability was as follows: MSC > SNV > CWT. In the RFR model simulation, the spectral performance capability was CWT > MSC > SNV. In the ANNR model simulation, the spectral performance ability was MSC > CWT > SNV. For the qP simulation, the spectral performance ability of the SVR model simulation was as follows: SNV > CWT > MSC. When the RFR model was simulated, the spectral performance ability was as follows: SNV > MSC > CWT. When the ANNR model was simulated, the spectral performance capability was as follows: CWT > SNV > MSC.

As shown in Table 7, considering the accuracy and error of modeling and verification, the optimal inversion model combinations of Fv/Fm and qP during the growth period of EF are the SVR model based on the MSC and the SVR model based on the SNV. The scatter plot of the optimal model is shown in Figure 7.

In Figure 7, the modeling R^2 values are 0.879 and 0.977, the verification R^2 values are 0.876 and 0.913, the modeling RMSE values are 0.005 and 0.007, the verification RMSE values are 0.008 and 0.015, the modeling RPD values are 2.774 and 6.417, and the verification RPD values are 1.535 and 2.997.
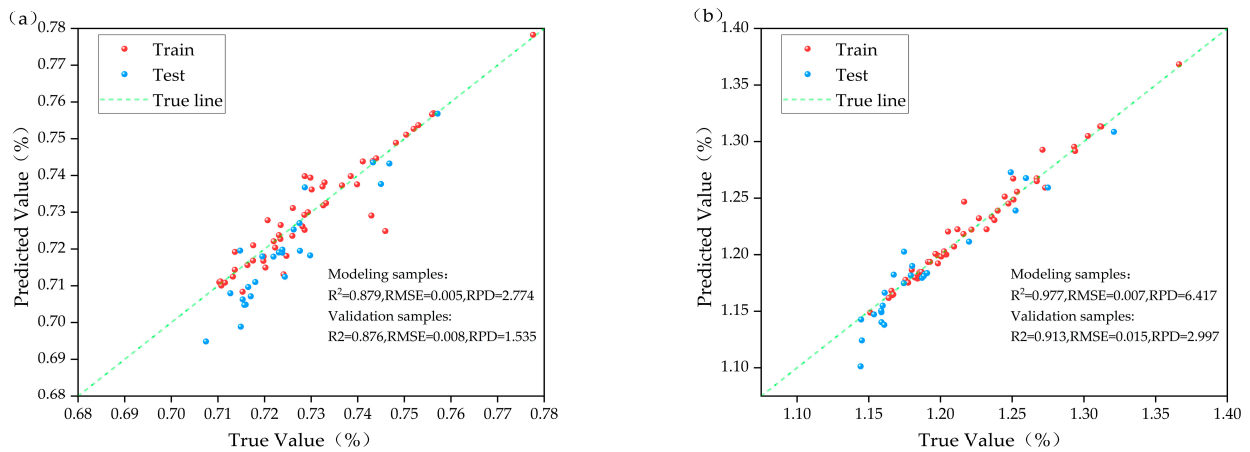
Figure 7. Scatter plots of the optimal simulated and measured values of Fv/Fm (**a**) and qP (**b**) during the FBS period.

In Table 8, during the EF growth period, the SVR model simulated Fv/Fm, and the spectral expression ability was CWT > SNV > MSC. In the RFR model simulation, the spectral performance capability was CWT > MSC > SNV. In the ANNR model simulation, the spectral performance capability was CWT > SNV > MSC. For the qP simulation, the spectral performance ability of the SVR model was as follows: CWT > MSC > SNV. When the RFR model was simulated, the spectral performance ability was as follows: CWT > SNV > MSC. When the ANNR model was simulated, the spectral performance ability was CWT > MSC > SNV.

As shown in Table 8, considering the accuracy and error of modeling and verification, the optimal inversion model combinations of Fv/Fm and qP during EF fertility are the CWT-based SVR model and the CWT-based SVR model, respectively. The scatter plot of the optimal model is shown in Figure 8.
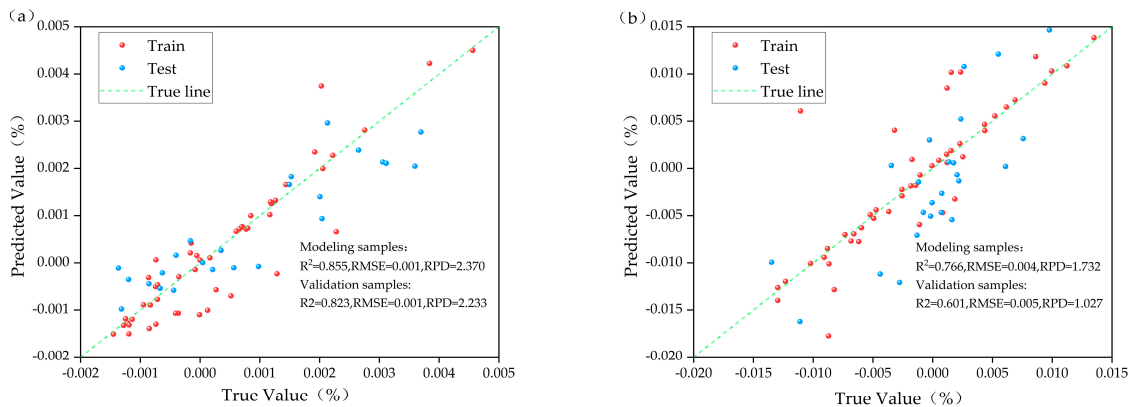
Figure 8. Scatter plots of the optimal simulated and measured values of Fv/Fm (**a**) and qP (**b**) during the PBP period.

In Figure 8, R^2 is modeled at 0.855 and 0.766, the verified R^2 values are 0.823 and 0.601, the modeled RMSE values are 0.001 and 0.004, the verified RMSE values are 0.001 and 0.005, the modeled RPD values are 2.370 and 1.732, and the verified RPD values are 2.233 and 1.027.

The results of the Fv/Fm and qP simulations revealed that the performance ability of the model was SVR > RF > ANN under the different irrigation amounts and different growth periods. The results show that it is feasible to simulate Fv/Fm via hyperspectra, but the effectiveness of simulated qP in the early flowering stage needs to be further verified.

4. Discussion

In the field of crop remote sensing monitoring, the extraction of characteristic spectral bands is always a key research topic, especially considering the problem of data redundancy. Traditionally, regression analysis has been performed on each band in multispectral data one by one to identify those characteristic bands that are sensitive to physiological and biochemical components of crops [34]. However, for hyperspectral data, an efficient algorithm is needed to accurately extract the feature information that is highly relevant to the target. In this study, CARS-SPA method was used to screen the characteristic bands, so as to realize the rapid extraction and analysis of spectral information. The fluorescence parameter Fv/Fm was mainly used to evaluate the photosynthetic capacity of plants and detect the stress status of plants, whereas qP was more focused on reflecting the efficiency of photochemical reactions and the light adaptation ability of plants. Among the characteristic bands selected via the CARS-SPA method, the blue and red bands had different effects on the photosynthesis of cotton, and a change in light quality led to fluctuations in the qP value and subsequently affected the growth and development of plants. These two parameters can provide key data for an in-depth understanding of plant photosynthesis mechanisms and their response to water stress. In this study, the two fluorescence parameters were inverted through a variety of pretreatment techniques and models to determine the best model. SVR, RFR, and ANNR have advantages and disadvantages: SVR has a strong ability to address nonlinear problems, but the calculation is complicated; RFR is easy to implement and can handle high-dimensional data but may overfit; and ANNR has strong modeling ability but complex training and poor interpretability.

The value of Fv/Fm is affected by many factors, such as light intensity, temperature, water conditions, chlorophyll content, PSII activity, and nutrients. qP is affected by light intensity, the CO_2 concentration, the composition of the photosynthetic pigment and protein complex, the state of the electron transport chain, and photorespiration. In addition, the stress conditions and developmental stages of plants also affect these parameters. Both Fv/Fm and qP play important roles in the study of plant physiology. Through significance level analysis, we found a correlation between Fv/Fm and qP and irrigation volume. With increasing irrigation amount, the Fv/Fm ratio usually first increased but then decreased, whereas the qP ratio first decreased but then increased in this experiment. In this study, the change trend of Fv/Fm value with growth period is different from that of previous studies [35], while the change trend of qP value showing first decrease and then increase is the same as that of previous studies [36]. The reason may be that FV/FM is more sensitive to moisture response and therefore has higher modeling accuracy. Under drought stress, the value of FV/FM will also decrease as the moisture content of cotton fields decreases gradually.

The results showed that SVR was superior to RFR and ANNR in simulating Fv/Fm and qP, whereas RFR was slightly superior to ANNR. The three models had better performance in terms of Fv/Fm inversion, indicating that hyperspectral data have a lower ability to interpret qP. However, the chlorophyll fluorescence parameters of each growth period can be retrieved on the optimal model. In application, the contents of Fv/Fm and qP can be determined via hyperspectral measurements, and then, the current stage of water stress can be analyzed to provide a basis for irrigation. To address this, future research should consider the potential integration of hyperspectral data with other remote sensing techniques (e.g., thermal imaging and LiDAR) as well as environmental factors (e.g., soil type and climate conditions) to provide a more comprehensive understanding of plant health and stress states. The current test results are limited because they do not consider many influencing factors, and it is recommended that these results be used only in regions with similar climatic conditions.

5. Conclusions

In this study, the Fv/Fm, qP, and hyperspectral reflectance of cotton canopy leaves at different growth stages were obtained on the basis of fluorescence parameters and

hyperspectral field experiments of cotton canopy leaves under different water treatments. Through the comparative analysis of the hyperspectral inversion results of the fluorescence parameters of the canopy leaves of the two cotton canopies, achieved by comparing and analyzing the results of the three spectra and three simulation methods, it was found that the Fv/Fm could be well simulated by hyperspectra, whereas the ability of hyperspectra to interpret the qP was low, which needs to be further studied. Hyperspectral information is strongly sensitive to the fluorescence parameters of cotton canopy leaves and can be used to monitor the moisture status of cotton and provide a theoretical basis because of the influence of spectral types and simulation methods.

References

1. Abdelraheem, A.; Esmaeili, N.; O'Connell, M.; Zhang, J. Progress and perspective on drought and salt stress tolerance in cotton. *Ind. Crops Prod.* **2019**, *130*, 118–129. [CrossRef]
2. Hikosaka, K.; Tsujimoto, K. Linking remote sensing parameters to CO_2 assimilation rates at a leaf scale. *J. Plant Res.* **2021**, *134*, 695–711. [CrossRef] [PubMed]
3. Murchie, E.; Lawson, T. Chlorophyll fluorescence analysis: A guide to good practice and understanding some new applications. *J. Exp. Bot.* **2013**, *64*, 3983–3998. [CrossRef] [PubMed]
4. Qin, S.; Ding, Y.; Zhou, Z.; Zhou, M.; Wang, H.; Xu, F.; Yao, Q.; Lv, X.; Zhang, Z.; Zhang, L. Study on the nitrogen content estimation model of cotton leaves based on "image-spectrum-fluorescence" data fusion. *Front. Plant Sci.* **2023**, *14*, 1117277. [CrossRef] [PubMed]
5. Strachan, I.; Pattey, E.; Salustro, C.; Miller, J. Use of hyperspectral remote sensing to estimate the gross photosynthesis of agricultural fields. *Can. J. Remote Sens.* **2008**, *34*, 333–341. [CrossRef]
6. Lobato, A.; Gonçalves-Vidigal, M.; Vidigal Filho, P.; Andrade, C.; Kvitschal, M.; Bonato, C. Relationships between leaf pigments and photosynthesis in common bean plants infected by anthracnose. *N. Z. J. Crop Hortic. Sci.* **2010**, *38*, 29–37. [CrossRef]
7. Croft, H.; Chen, J.; Wang, R.; Mo, G.; Luo, S.; Luo, X.; He, L.; Gonsamo, A.; Arabian, J.; Zhang, Y. The global distribution of leaf chlorophyll content. *Remote Sens. Environ.* **2020**, *236*, 111479. [CrossRef]
8. Li, Y.; Ma, Q.; Chen, J.; Croft, H.; Luo, X.; Zheng, T.; Rogers, C.; Liu, J. Fine-scale leaf chlorophyll distribution across a deciduous forest through two-step model inversion from Sentinel-2 data. *Remote Sens. Environ.* **2021**, *264*, 112618. [CrossRef]
9. Richardson, A.; Duigan, S.; Berlyn, G. An evaluation of noninvasive methods to estimate foliar chlorophyll content. *New Phytol.* **2002**, *153*, 185–194. [CrossRef]
10. Ali, A.; Imran, M. Remotely sensed real-time quantification of biophysical and biochemical traits of Citrus (*Citrus sinensis* L.) fruit orchards–A review. *Sci. Hortic.* **2021**, *282*, 110024. [CrossRef]
11. Kokaly, R.F.; Asner, G.; Ollinger, S.; Martin, M.; Wessman, C. Characterizing canopy biochemistry from imaging spectroscopy and its application to ecosystem studies. *Remote Sens. Environ.* **2009**, *113*, S78–S91. [CrossRef]
12. Peterson, R.; Sivak, M.; Walker, D. Relationship between steady-state fluorescence yield and photosynthetic efficiency in spinach leaf tissue. *Plant Physiol.* **1988**, *88*, 158–163. [CrossRef] [PubMed]
13. Pérez-Priego, O.; Zarco-Tejada, P.; Miller, J.; Sepulcre-Cantó, G.; Fereres, E. Detection of water stress in orchard trees with a high-resolution spectrometer through chlorophyll fluorescence in-filling of the O/sub 2/-A band. *IEEE Trans. Geosci. Remote Sens.* **2005**, *43*, 2860–2869. [CrossRef]
14. Ding, Y.; Qin, S.; Ma, L.; Chen, X.; Yao, Q.; Yang, M.; Ma, Y.; Lv, X.; Zhang, Z. A study on cotton yield prediction based on the chlorophyll fluorescence parameters of upper leaves. *Not. Bot. Horti Agrobot. Cluj-Napoca* **2022**, *50*, 12775. [CrossRef]

15. Prasad, A.; Chai, L.; Singh, R.; Kafatos, M. Crop yield estimation model for Iowa using remote sensing and surface parameters. *Int. J. Appl. Earth Obs. Geoinf.* **2006**, *8*, 26–33. [CrossRef]
16. Blackburn, G. Hyperspectral remote sensing of plant pigments. *J. Exp. Bot.* **2007**, *58*, 855–867. [CrossRef]
17. Nigam, R.; Kot, R.; Sandhu, S.; Bhattacharya, B.; Chandi, R.; Singh, M.; Singh, J.; Manjunath, K. Ground-based hyperspectral remote sensing to discriminate biotic stress in cotton crop. In *Multispectral, Hyperspectral, and Ultraspectral Remote Sensing Technology, Techniques and Applications VI*; SPIE: Bellingham, WA, USA, 2016; Volume 9880, pp. 89–98.
18. Gläßer, C.; Groth, D.; Frauendorf, J. Monitoring of hydrochemical parameters of lignite mining lakes in Central Germany using airborne hyperspectral casi-scanner data. *Int. J. Coal Geol.* **2011**, *86*, 40–53. [CrossRef]
19. Fu, D.; Zhou, J.; Scaboo, A. Fast measurement of fatty acid in soybean using reflective hyperspectral imaging. In *2019 ASABE Annual International Meeting*; American Society of Agricultural and Biological Engineers: St. Joseph, MI, USA, 2019; p. 1.
20. Sun, J.; Wang, G.; Zhang, H.; Xia, L.; Zhao, W.; Guo, Y.; Sun, X. Detection of fat content in peanut kernels based on chemometrics and hyperspectral imaging technology. *Infrared Phys. Technol.* **2020**, *105*, 103226. [CrossRef]
21. Zarco-Tejada, P.; Miller, J.; Mohammed, G.; Noland, T. Chlorophyll fluorescence effects on vegetation apparent reflectance: I. Leaf-level measurements and model simulation. *Remote Sens. Environ.* **2000**, *74*, 582–595. [CrossRef]
22. Chaerle, L.; Hagenbeek, D.; De Bruyne, E.; Valcke, R.; Van Der Straeten, D. Thermal and chlorophyll-fluorescence imaging distinguish plant-pathogen interactions at an early stage. *Plant Cell Physiol.* **2004**, *45*, 887–896. [CrossRef]
23. Zhang, H.; Hu, H.; Zhang, X.; Wang, K.; Song, T.; Zeng, F. Detecting Suaeda salsa L. chlorophyll fluorescence response to salinity stress by using hyperspectral reflectance. *Acta Physiol. Plant.* **2012**, *34*, 581–588. [CrossRef]
24. Winkel, T.; Méthy, M.; Thénot, F. Radiation use efficiency, chlorophyll fluorescence, and reflectance indices associated with ontogenic changes in water-limited Chenopodium quinoa leaves. *Photosynthetica* **2002**, *40*, 227–232. [CrossRef]
25. Demmig-Adams, B.; Adams, W., III; Barker, D.; Logan, B.; Bowling, D.; Verhoeven, A. Using chlorophyll fluorescence to assess the fraction of absorbed light allocated to thermal dissipation of excess excitation. *Physiol. Plant.* **1996**, *98*, 253–264. [CrossRef]
26. Evans, J. Improving photosynthesis. *Plant Physiol.* **2013**, *162*, 1780–1793. [CrossRef] [PubMed]
27. Wu, S.; Amari, S. Conformal transformation of kernel functions: A data-dependent way to improve support vector machine classifiers. *Neural Process. Lett.* **2002**, *15*, 59–67. [CrossRef]
28. Chen, X.; Li, F.; Shi, B.; Fan, K.; Li, Z.; Chang, Q. Estimation of winter wheat canopy chlorophyll content based on canopy spectral transformation and machine learning method. *Agronomy* **2023**, *13*, 783. [CrossRef]
29. Park, D.; El-Sharkawi, M.; Marks, R.; Atlas, L.; Damborg, M. Electric load forecasting using an artificial neural network. *IEEE Trans. Power Syst.* **1991**, *6*, 442–449. [CrossRef]
30. Yue, J.; Feng, H.; Yang, G.; Li, Z. A comparison of regression techniques for estimation of above-ground winter wheat biomass using near-surface spectroscopy. *Remote Sens.* **2018**, *10*, 66. [CrossRef]
31. Liu, J.; Dong, Z.; Xia, J.; Wang, H.; Meng, T.; Zhang, R.; Han, J.; Wang, N.; Xie, J. Estimation of soil organic matter content based on CARS algorithm coupled with random forest. *Spectrochim. Acta Part A Mol. Biomol. Spectrosc.* **2021**, *258*, 119823. [CrossRef]
32. Fu, L.; Li, P.; Gao, L. Improved least squares support vector machine algorithm considering sample outliers. *Chin. J. Sci. Instrum.* **2023**, *6*, 179–190. (In Chinese)
33. Gao, S.; Wang, Q. Non-destructive testing of red sugar content and water content based on visible/near-infrared transmission spectroscopy. *Chin. Opt. (Engl. Chin.)* **2021**, *14*, 566–577. (In Chinese)
34. Ma, L.; Chen, X.; Zhang, Q.; Lin, J.; Yin, C.; Ma, Y.; Yao, Q.; Feng, L.; Zhang, Z.; Lv, X. Estimation of Nitrogen Content Based on the Hyperspectral Vegetation Indexes of Interannual and Multi-Temporal in Cotton. *Agronomy* **2022**, *12*, 1319. [CrossRef]
35. Lin, X.; Ha, F.; Ma, L.; Chen, X.; Ma, Y.; Chen, A.; Hou, Z.; Zhang, Z. A cotton leaf nitrogen monitoring model based on spectral-fluorescence data fusion. *Not. Bot. Horti Agrobot. Cluj-Napoca* **2023**, *51*, 13059. [CrossRef]
36. Liu, J.; Wang, Y.; Gao, S.; Jiang, W. Study on the Effect of Interspecific Hybridization Island Cotton Varities on the Chloro Phyll Fluoreseence Parameters and Physiological Biochemistry Dynamic Change. *Seed* **2012**, *31*, 4–9. (In Chinese)